

Research Article

Localized Effects in Periodic Elastoplastic Composites

Jacob Aboudi* and Michael Ryvkin

Department of Engineering, Tel Aviv University, Israel

***Corresponding author:** Jacob Aboudi, Department of Engineering, School of Mechanical Engineering, Tel Aviv University, Ramat Aviv 69978, Israel**Received:** November 24, 2014; **Accepted:** February 14, 2015; **Published:** February 18, 2015**Abstract**

A method is applied for the study of the field distributions in metal matrix fiber reinforced composites with periodic microstructure in which localized damage exists in the form of complete or partial fiber loss and crack. In addition, the behavior of ceramic/metal periodically layered composites with a single broken ceramic layer is determined. The proposed analysis is based on continuum damage mechanics considerations, and the method of solution combines three distinct approaches. In the first one, referred to as the representative cell method, the periodic composite domain is reduced, in conjunction with the discrete Fourier transform to a finite domain problem of a single representative cell. This method has been previously applied on linear thermoelastic, smart and electrostrictive composites, but is presently extended and applied on elastoplastic composites (presently deformation and incremental plasticity). In the second approach, the appropriate far-field boundary conditions in the transform domain are applied in conjunction with the high-fidelity generalized method of cells micromechanical model for the prediction of the macroscopic behavior of the inelastic composite. The third approach consists of the application of the inelastic higher-order theory for the computation of the elastoplastic field in the transform domain. An inverse transform provides the actual field. The effect of damage is included in the analysis in the form of eigenstresses which are a priori unknown. Hence an iterative procedure is employed to obtain a convergent solution.

The proposed method is verified by a comparison with an analytical solution, and several applications illustrate the applicability of the method for metal matrix composites with localized damage in the form of a crack or fiber loss.

Keywords: Localized damage; Cracked fiber reinforced materials; Representative cell method; High-Fidelity generalized method of cells; Inelastic higher-order theory; Elastoplastic composites

Introduction

The micromechanical analysis of composites with periodic microstructure is usually carried out by identifying and analyzing a repeating unit cell. However, when localized effects such as one or several cracks occur in the composite, the periodicity is lost and its behavior cannot be determined directly by analyzing a repeating unit cell. If these effects are nevertheless included in the analysis of the repeating unit cell, the resulting behavior would correspond to that of a composite with periodic (i.e., not localized) effects which obviously is an unrealistic situation.

In a recent article, Aboudi and Ryvkin [1] proposed the analysis of linearly elastic composites with localized damage by representing the effect of the latter by eigenstresses. This analysis combines continuum damage mechanics considerations with three different approaches. In the first one the idea of using the eigenstresses to represent the nonlinear effects enables application of the representative cell method, Ryvkin and Nuller [2], based on the discrete Fourier transform which is applicable to linear problems. As a result the initial problem formulated for a domain comprising a large number of cells is reduced to a problem for a single representative cell. Appropriate far-field boundary conditions (which are not influenced by the localized effects) in the transform domain are applied in conjunction with the high-fidelity generalized method of cells (HFGMC) [3] micromechanical model which forms the second approach. The third approach consists

of the application of the higher-order inelastic theory, Aboudi et al. [4], for the computation of the field in the transform domain. An inverse transform provides the actual field. The effect of damage is included in the analysis in the form of eigenstresses which are a priori unknown. In Ryvkin and Aboudi [5], this approach has been also proven to be successful and effective in the analysis of cracked layered elastic composites, where one or several combinations of a transverse and two longitudinal cracks (H-cracks) caused branching have been investigated. Furthermore, it has been successfully applied for the prediction of the field distributions in electro-magneto-thermo-elastic composites with cracks, cavities and inclusions, Aboudi [6]. A brief review of various methods for the analysis of localized effects in thermoelastic composites has been recently presented by Aboudi and Ryvkin [3].

Thus far, the representative cell method has been employed in the analysis of linearly thermoelastic [1], electro-magneto-thermo-elastic [6] and electrostrictive (nonlinear) [7] composites. In the present investigation, this method is extended to elastoplastic materials (presently incremental and deformation elastoplasticity). In addition, the approach of Aboudi and Ryvkin [1] in analyzing localized damage in composites is presently further extended to enable the prediction of the behavior of elastoplastic periodic composites which include localized damage in the form of a cavity (a fiber loss) or a crack. In this approach, the plasticity effects are represented in the form of eigenstresses which extend over the entire considered region. In

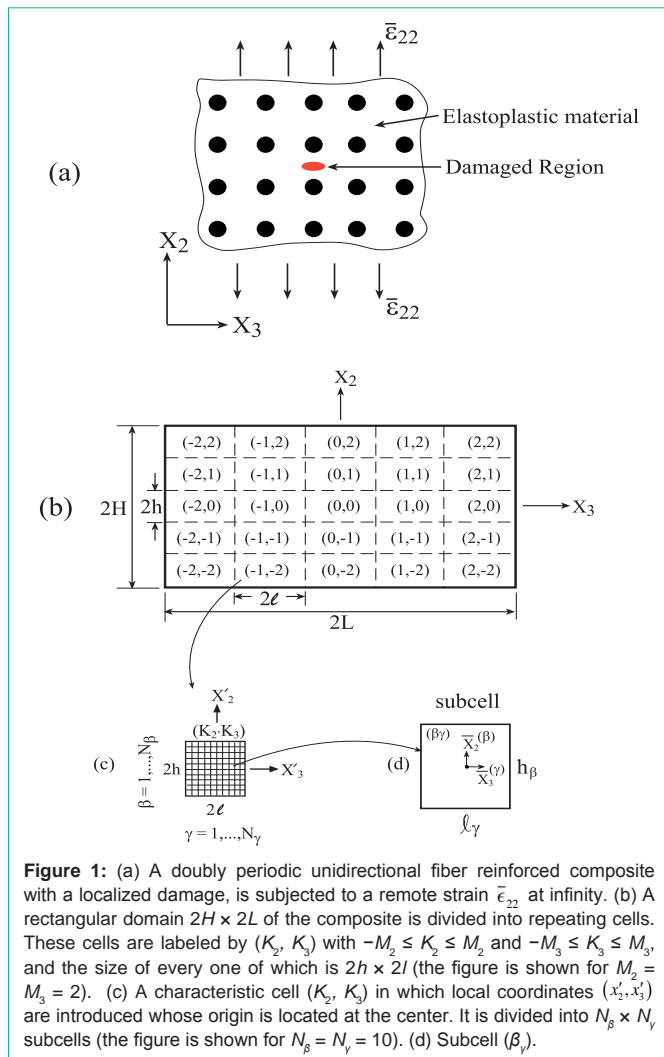


Figure 1: (a) A doubly periodic unidirectional fiber reinforced composite with a localized damage, is subjected to a remote strain $\bar{\epsilon}_{22}$ at infinity. (b) A rectangular domain $2H \times 2L$ of the composite is divided into repeating cells. These cells are labeled by (K_2, K_3) with $-M_2 \leq K_2 \leq M_2$ and $-M_3 \leq K_3 \leq M_3$, and the size of every one of which is $2h \times 2l$ (the figure is shown for $M_2 = M_3 = 2$). (c) A characteristic cell (K_2, K_3) in which local coordinates (x'_2, x'_3) are introduced whose origin is located at the center. It is divided into $N_\beta \times N_\gamma$ subcells (the figure is shown for $N_\beta = N_\gamma = 10$). (d) Subcell $(\beta\gamma)$.

addition, these eigenstresses include the effects of localized damage which are operative over the damaged region only as has been proposed by Aboudi and Ryvkin [1] in the case of linear elasticity. Thus, according to our present proposed approach these eigenstresses include the combined contributions of the effects of plasticity as well as the localized damage. These eigenstresses are not known in advance and, therefore, an iterative procedure is employed to establish a convergent solution.

This article is organized as follows. In the next section the problem is formulated which followed by the method of solution section. The verification of the method is performed by a comparison with analytical solution for an infinite elastoplastic (deformation plasticity) medium with embedded cavity subjected to a remote biaxial loading, Ishikawa [8]. The application section presents the applicability of the proposed method for the prediction of the behavior of elastoplastic solids with embedded cavity, fiber reinforced metal matrix composites with a complete and partial fiber loss, and layered metal matrix composite with a single broken layer. The final section presents the conclusions and several possible future generalizations.

Problem Statement

The present investigation deals with elastoplastic composites

that possess a periodic microstructure and include a localized damage such as a crack, fiber loss or cavity. This type of composites is illustrated in Figure 1(a) where the fibers, oriented in the x_1 -direction and arranged in a doubly periodic manner, are embedded in an elastoplastic material.

The response of the considered composite is determined by satisfying the equilibrium equations in every one of its constituents, namely:

$$\nabla \cdot \sigma = 0 \tag{1}$$

in the absence of body forces, where σ is the stress tensor. In addition, the interfacial conditions that requires in the case of perfect bonding the continuity of displacements u and tractions t between the fibers (f) and matrix (m) constituents must be imposed:

$$u^f = u^m, t^f = t^m \tag{2}$$

In the present investigation elastoplastic materials are considered whose constitutive equations are given (assuming isothermal conditions) by

$$\sigma = C: (\epsilon - \epsilon^p) \tag{3}$$

where C is the stiffness tensor of the material, and ϵ and ϵ^p are the strain and plastic strain tensors, respectively. In the framework of classical plasticity, the evolution law of the plastic strain ϵ^p is governed by the Prandtl-Reuss equations, c.f. Mendelson [9]:

$$\Delta \epsilon^p = \Delta \lambda s \tag{4}$$

where $\Delta \lambda$ is the Prandtl-Reuss proportionality function and s is the deviator tensor of σ .

In Aboudi and Ryvkin [1], the effect of localized damage in perfectly elastic composites was represented by eigenstresses as follows. The constitutive equations of elastic material in the presence of damage are determined by the principle of strain equivalence Lemaitre and Desmorat [10], according to which the strains in the damaged and effective configurations are equal. This implies that

$$\sigma = C: \epsilon - \sigma^e \tag{5}$$

where σ^e is eigenstress which has the form

$$\sigma^e = DC: \epsilon \tag{6}$$

where D is the damage variable which is equal to zero in the undamaged constituents, whereas $D = 1$ in cracks and cavity regions thus representing a complete damage. In addition to the contribution of Aboudi and Ryvkin [1] where this method was presented and applied to investigate localized damage in elastic composites, this approach has been also shown to be successful in the modeling of an H-crack (a transverse crack accompanied by two longitudinal ones) in ceramic matrix composites Ryvkin and Aboudi [5], and cracks, cavities and inclusions in electro-magneto-elastic composites Aboudi [6].

In the present paper where the constitutive equations of the phases incorporate inelastic effects we propose to continue representing the constitutive equations by Equation (5) but generalize Equation (6) as follows

$$\sigma^e = DC: \epsilon + (I-D)C: \epsilon^p \tag{7}$$

Thus, the eigenstresses presently include the plasticity effects in addition to the damage. It should be noted that in the absence of damage ($D = 0$) the plasticity effects are included in the analysis in the form of eigenstresses and their effects extend over the entire region. In the presence of damage in certain localized regions ($0 < D < 1$) further terms are added to the latter. In regions with complete damage ($D = 1$) where cracks and cavities are simulated, the plasticity effects as expected are absent. It can be readily observed that with introduction of the damage parameter D , it is possible to model a region whose behavior is elastoplastic everywhere except for one or more localized domains where $D = 1$ which corresponds to cavities and cracks. Evolving damage, stiff and soft inclusions, where D takes suitable values between zero and one have been utilized in the modeling of thermoelastic, electro-magneto-thermo-elastic and electrostrictive composites, see Aboudi and Ryvkin [1], Aboudi [6] and Aboudi [7], respectively.

Finally, as it is discussed in the next section, the far-field boundary conditions that are applied on the composite should be incorporated.

Method of Solution

Far away from the region with localized damage, the periodic elastoplastic composite is governed at any instant of loading by its macroscopic (global) behavior. The constitutive equations that model this behavior can be micromechanically established by the HFGMC model, Aboudi et al. [4] chapter 6, and are given by

$$\bar{\sigma} = C^* : (\bar{\epsilon} - \bar{\epsilon}^p) \tag{8}$$

where C^* is the effective stiffness tensor and $\bar{\sigma}$, $\bar{\epsilon}$ and $\bar{\epsilon}^p$ are the global stress, total strain and plastic strain tensors, respectively.

Let us consider a rectangular domain $-H \leq x_2 \leq H, -L \leq x_3 \leq L$ of the composite which includes the damaged region. Although this region includes the localized damage, it is assumed that it is extensive enough such that the inelastic stress, strain and displacement fields at its boundaries are not influenced by the damage existence and therefore, the macroscopic constitutive equations (8) are applicable. Consequently, the boundary conditions that are applied on $x_2 = \pm H$ and $x_3 = \pm L$ are referred to as the far-field boundary conditions. According to the representative cell method, Ryvkin and Nuller [2], this region is divided into $(2M_2 + 1) \times (2M_3 + 1)$ identical cells, see Figure 1(b) which is schematically shown for $M_2 = M_3 = 2$ cells. Every cell is labeled by (K_2, K_3) with $K_2 = -M_2, \dots, M_2$ and $K_3 = -M_3, \dots, M_3$. In each cell, local coordinates (x'_2, x'_3) are introduced whose origins are located at its center, see Figure 1(c) which shows the representative cell that is schematically divided into $N_\beta = 10$ and $N_\gamma = 10$ subcells.

The equilibrium equation (1) of the materials within the cell (K_2, K_3) takes the form

$$\nabla \cdot \sigma^{(K_2, K_3)} = 0 \tag{9}$$

The constitutive equation in the cell, Equation (5), can be written as

$$\sigma^{(K_2, K_3)} = C : \epsilon^{(K_2, K_3)} - \sigma^e(K_2, K_3) \tag{10}$$

where the eigenstresses in cell (K_2, K_3) are given according to Equation (6) by

$$\sigma^e(K_2, K_3) = DC : \epsilon^{(K_2, K_3)} + (1 - D)C : \epsilon^p(K_2, K_3) \tag{11}$$

and

$$D = \begin{cases} 0 & \text{no damage} \\ 1 & \text{full damage} \end{cases} \tag{12}$$

and $0 < D < 1$ for a partial damage.

The continuity of displacements $u(K_2, K_3)$ and tractions $t(K_2, K_3)$ between adjacent cells should be imposed. Thus,

$$[u(h, x'_3)]^{(K_2, K_3)} - [u(-h, x'_3)]^{(K_2+1, K_3)} = 0 \tag{13}$$

$$[t^{(2)}(h, x'_3)]^{(K_2, K_3)} - [t^{(2)}(-h, x'_3)]^{(K_2+1, K_3)} = 0 \tag{14}$$

where $K_2 = -M_2, \dots, M_2 - 1, K_3 = -M_3, \dots, M_3 - l \leq x'_3 \leq l$, and

$$[u(x'_2, l)]^{(K_2, K_3)} - [u(x'_2, -l)]^{(K_2, K_3+1)} = 0 \tag{15}$$

$$[t^{(3)}(x'_2, l)]^{(K_2, K_3)} - [t^{(3)}(x'_2, -l)]^{(K_2, K_3+1)} = 0 \tag{16}$$

where $K_2 = -M_2, \dots, M_2, K_3 = -M_3, \dots, M_3 - 1, -h \leq x'_2 \leq h$. Here $t^{(j)}$ is the traction vector acting at a boundary perpendicular to the x_j -axis, $j = 2, 3$.

In the following, the appropriate form of the far-field boundary conditions that specify the tractions and displacements at the opposite sides $x_2 = \pm H, x_3 = \pm L$ of the rectangle of Figure 1(b) are presented. The tractions at the opposite sides of the rectangular domain are equal:

$$[t^{(2)}]^{(M_2, K_3)}(h, x'_3) - [t^{(2)}]^{(-M_2, K_3)}(-h, x'_3) = 0, \quad K_3 = -M_3, \dots, M_3, \quad -l \leq x'_3 \leq l \tag{17}$$

$$[t^{(3)}]^{(K_2, M_3)}(x'_2, l) - [t^{(3)}]^{(K_2, -M_3)}(x'_2, -l) = 0, \quad K_2 = -M_2, \dots, M_2, \quad -h \leq x'_2 \leq h \tag{18}$$

The displacements at the opposite sides, on the other hand, differ by certain jumps as follows

$$u^{(M_2, K_3)}(h, x'_3) - u^{(-M_2, K_3)}(-h, x'_3) = \delta_2, \quad K_3 = -M_3, \dots, M_3, \quad -l \leq x'_3 \leq l \tag{19}$$

$$u^{(K_2, M_3)}(x'_2, l) - u^{(K_2, -M_3)}(x'_2, -l) = \delta_3, \quad K_2 = -M_2, \dots, M_2, \quad -h \leq x'_2 \leq h \tag{20}$$

where δ_2 and δ_3 denote the vectors of the far-field displacement differences whose components are given by

$$\delta_{2j} = 2H\bar{\epsilon}_{2j}, \quad \delta_{3j} = 2L\bar{\epsilon}_{3j}, \quad j=1,2,3 \tag{21}$$

and $\bar{\epsilon}_{2j}, \bar{\epsilon}_{3j}$ are the macroscopic (global) strains of the unperturbed periodic composite which have to be determined from Equation (8) for a given type of applied loading. Suppose, for example, that the composite is subjected to a transverse strain loading

$\bar{\epsilon}_{22}$ with $\bar{\sigma}_{ij} = 0$ in all other directions. The macroscopic equations (8) that describe the (undamaged) composite's behavior are utilized to determine the remaining average strains $\bar{\epsilon}_{ij}, i, j \neq 2$ to be employed in Equation (21).

The double finite discrete Fourier transform of the displacement vector $u^{(K_2, K_3)}$, for example, is defined by

$$\hat{u}(x'_2, x'_3, \phi_p, \phi_q) = \sum_{K_2=-M_2}^{M_2} \sum_{K_3=-M_3}^{M_3} u^{(K_2, K_3)}(x'_2, x'_3) \exp[i(K_2\phi_p + K_3\phi_q)] \tag{22}$$

where

$$\phi_p = \frac{2\pi p}{2M_2 + 1}, \quad p = 0, \pm 1, \pm 2, \dots, \pm M_2, \quad \phi_q = \frac{2\pi q}{2M_3 + 1}, \quad q = 0, \pm 1, \pm 2, \dots, \pm M_3,$$

The application of this transform to the boundary value problem (9)-(20) for the rectangular domain $-H < x_2 < H, -L < x_3 < L$, divided into $(2M_2 + 1) \times (2M_3 + 1)$ cells, converts it to the problem for the single representative cell $-h < x'_2 < h, -l < x'_3 < l$ with respect to the complex valued transforms. The field equations obtained from the equilibrium and constitutive equations have the form

$$\nabla \cdot \hat{\sigma} = 0 \tag{23}$$

and

$$\hat{\sigma} = C \hat{\epsilon} - \hat{\sigma}^e \tag{24}$$

where the transformed eigenstress tensor is given by

$$\hat{\sigma}^e = DC : \hat{\epsilon} + (1 - D)C : \hat{\epsilon}^p \tag{25}$$

The conditions relating the opposite boundaries of the representative cell in the elastic problem case were derived by Aboudi and Rvynkin [1]. Following their approach one obtains from (13)-(20)

$$\hat{u}(h, x'_3) = \exp(-i\phi_p)\hat{u}(-h, x'_3) + \delta_{0,q}(2M_3 + 1)\delta_2 \exp(i\phi_p M_2), \quad -l \leq x'_3 \leq l \tag{26}$$

$$\hat{t}^{(2)}(h, x'_3) = \exp(-i\phi_p)\hat{t}^{(2)}(-h, x'_3), \quad -l \leq x'_3 \leq l \tag{27}$$

and

$$\hat{u}(x'_2, l) = \exp(-i\phi_q)\hat{u}(x'_2, -l) + \delta_{0,p}(2M_2 + 1)\delta_3 \exp(i\phi_q M_3), \quad -h \leq x'_2 \leq h \tag{28}$$

$$\hat{t}^{(3)}(x'_2, l) = \exp(-i\phi_q)\hat{t}^{(3)}(x'_2, -l), \quad -h \leq x'_2 \leq h \tag{29}$$

where $p = -M_2, \dots, M_2; q = -M_3, \dots, M_3$. In these equations, $\delta_{p,q}$ denotes the Kronecker delta.

The representative cell boundary value problem (23)-(29) have been solved by employing the inelastic higher-order theory, Aboudi et al. (2013), chapter 11. According to this theory, the domain $-h \leq x'_2 \leq h, -l \leq x'_3 \leq l$ (the representative cell) is divided into $N_\beta \times N_\gamma$ rectangular subcells $\beta = 1, \dots, N_\beta, \gamma = 1, \dots, N_\gamma$, see Figure 1(c) where $N_\beta = N_\gamma = 10$. The transformed displacement vector is expanded into a second-order polynomial in the subcell (β, γ) , Figure 1(d), and the equilibrium equations, interfacial and boundary conditions are imposed in the average (integral) sense. In order to model a (line) crack, a single row of subcells filled with a fully damaged

($D = 1$) elastoplastic material is introduced. Thus the value of the damage variable D is pre-determined in accordance with the crack configuration. If on the other hand a cavity is modeled, then its entire elastoplastic region of subcells is modeled with $D = 1$.

Once the solution at a current instant of loading in the transform domain has been established, the actual elastoplastic field can be readily determined at any point in the desired cell (K_2, K_3) of the considered rectangular region $-H \leq x_2 \leq H, -L \leq x_3 \leq L$ by the inverse transform formula whose form for the displacements, for example, is:

$$u^{(K_2, K_3)}(x'_2, x'_3) = \frac{1}{(2M_2 + 1)(2M_3 + 1)} \tag{30}$$

$$\times \sum_{p=-M_2}^{M_2} \sum_{q=-M_3}^{M_3} \hat{u}(x'_2, x'_3, \phi_p, \phi_q) \exp[-i(K_2\phi_p + K_3\phi_q)]$$

In the application of this theory, the eigenstress tensor $\hat{\sigma}^e$, to be used in Equation (24) is not known. Hence an iterative solution has to be employed as shown in the flow chart.

This procedure should be continued until a convergence to a desired degree of accuracy is achieved. Having established the solution at the current increment, one can proceed to the next increment by a slight change of the applied loading.

Verification

In all cases given in this paper, the computations of the elastoplastic field were carried out with a square representative cell $h = l$, Figure 1(c). Which is discretized into 2500 subcells with $N_\beta = N_\gamma = 50$ subcells. The region $-H \leq x_2 \leq H, -L \leq x_3 \leq L$ has been divided into 289 cells with $M_2 = M_3 = 8$. This choice was verified in providing a periodic (unperturbed) field far away from the localized damage which was always taken to exist in cell $M_2 = M_3 = 0$ only. Thus, the use of global constitutive relations, Equation (8), for the determination of the far-field inelastic boundary conditions is justified.

The verification of the present approach has been performed by comparing the resulting response to a remote biaxial loading of an elastoplastic material with an embedded circular cavity. This problem has been originally investigated by Budiansky and Mangasarian [11]. The material is described by the Ramberg-Osgood deformation theory of plasticity which for a uniaxial stress-strain case is given by

$$\epsilon = \frac{\sigma}{E} + \frac{\alpha Y}{E} \left(\frac{\sigma}{Y} \right)^n \tag{31}$$

where E is the Young's modulus of the material, Y is its yield stress and α and n are material parameters. For elastic strains which are negligible compared to the plastic strains, Budiansky and Mangasarian [11] provided a closed-form expression for the material response in this special case. An analytical solution for arbitrary values of the elastic strains has been derived by Ishikawa [8]. This solution is presently employed for comparison with the proposed analysis to verify our approach.

The uniaxial stress-strain Ramberg-Osgood relation (31) can be generalized to a multiaxial one yielding

$$\epsilon_{ij} = \frac{1+\nu}{E} \sigma_{ij} - \frac{\nu}{E} \sigma_{kk} \delta_{i,j} + \frac{3\alpha}{2E} \left(\frac{\sigma_{eq}}{Y} \right)^{n-1} s_{ij} \tag{32}$$

where ν is the Poisson's ratio of the material and the equivalent stress is defined by $\sigma_{eq} = \sqrt{3s_{ij}s_{ij}/2}$ with s_{ij} being the deviators of the stresses σ_{ij} . This equation can be inverted (R. Haj-Ali, personal communication) to yield (see Appendix for a proof):

$$\sigma_{ij} = K \epsilon_{ik} \delta_{i,j} + \frac{e_{ij}}{\frac{1}{2G} + \frac{3\alpha}{2E} \left(\frac{\sigma_{eq}}{Y}\right)^{n-1}} \quad (33)$$

where K, G are the bulk and shear moduli and σ_{eq} is the root of the following nonlinear equation

$$\frac{3\alpha Y}{2E} \left(\frac{\sigma_{eq}}{Y}\right)^n + \frac{Y}{2G} \left(\frac{\sigma_{eq}}{Y}\right) - e_{eq} = 0 \quad (34)$$

In these equations, $e_{eq} = \sqrt{3e_{ij}e_{ij}/2}$ with e_{ij} being the deviators of the strain components ϵ_{ij} . Consequently, in the present case Equation (4) should be replaced by

$$\epsilon^p = \frac{3\alpha}{2E} \left(\frac{\sigma_{eq}}{Y}\right)^{n-1} s \quad (35)$$

With $\alpha = 3/7$, the analytical solution of Ishikawa [8], expressed in polar coordinates (r, θ) located at the cavity center whose radius is a , is based for plane stress conditions and remote biaxial loading on the following nonlinear equation

$$\frac{3}{7} \left[\frac{1}{4} \left(\frac{a}{r}\right)^2 + \frac{1}{12} \right]^{(n-1)/2} (\sqrt{3\xi})^{n-1} \left(\frac{2r^2}{r^2+a^2} s_{\theta\theta} \right)^n + \frac{2r^2}{r^2+a^2} s_{\theta\theta} - 2 \left(1 + \frac{3}{7} \xi^{n-1} \right) = 0 \quad (36)$$

where $\xi = \bar{\sigma}_{rr}/Y$ being the applied remote radial stress $\bar{\sigma}_{rr}$ normalized with respect to the yield stress Y , and $s_{\theta\theta} = \sigma_{\theta\theta}/\bar{\sigma}_{rr}$. Once the root $s_{\theta\theta}$ of this equation for an applied value of ξ is determined, the value of σ_{rr} is evaluated from

$$\sigma_{rr} = \frac{1-a^2}{1+a^2} \sigma_{\theta\theta}$$

It should be noted that Ishikawa [8] solution is independent of the elastic parameters of the material.

The comparison between variations along x_3 at $x_2 = 0$ of $\sigma_{22} \equiv \sigma_{\theta\theta}$ and $\sigma_{33} \equiv \sigma_{rr}$ as predicted by the present approach and Ishikawa [8] analytical solution is shown in Figure 2 for a cavity radius of $a/(2h) = 0.28$. For a nonlinear epoxy, the material properties are given by Table 1 and the loading is given by $\bar{\epsilon}_{22} = \bar{\epsilon}_{33}$ which is incrementally increased up to the value of $\bar{\epsilon}_{22} = \bar{\epsilon}_{33} = 1.8\%$. Plane stress condition is assumed in the present case such that $\sigma_{11} = 0$ everywhere. This final value of applied strain corresponds to a far-field stress of $\bar{\sigma}_{22} = \bar{\sigma}_{33} = 142\text{MPa}$ (which is slightly below the yield stress $Y = 157.6\text{MPa}$). The figure shows comparisons between the analytical and the present solutions at far-field loading of $\bar{\epsilon}_{22} = \bar{\epsilon}_{33} = 1.2\%$ (which corresponds to $\bar{\sigma}_{22} = \bar{\sigma}_{33} = 95.6\text{MPa}$) and at $\bar{\epsilon}_{22} = \bar{\epsilon}_{33} = 1.8\%$. Very good agreements between the two solutions can be observed (the radial stress variations coincide). As can be expected, the equivalent plastic strain ϵ_{eq}^p attains its maximum value at the $r = a$ and rapidly decays with increasing r . The maximum values of ϵ_{eq}^p obtained from the applied far-field of 1.2% and 1.8% are 1.7% and 5.3%, respectively.

It should be noted that the selection of $M_2 = M_3 = 8$ as the number

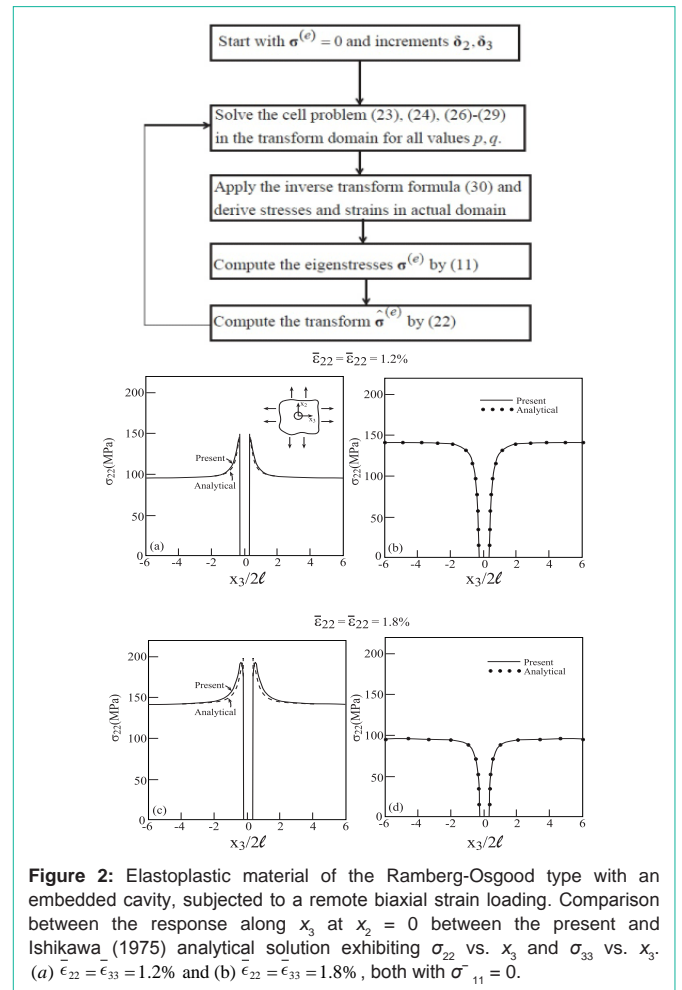


Figure 2: Elastoplastic material of the Ramberg-Osgood type with an embedded cavity, subjected to a remote biaxial strain loading. Comparison between the response along x_3 at $x_2 = 0$ between the present and Ishikawa (1975) analytical solution exhibiting σ_{22} vs. x_3 and σ_{33} vs. x_3 . (a) $\bar{\epsilon}_{22} = \bar{\epsilon}_{33} = 1.2\%$ and (b) $\bar{\epsilon}_{22} = \bar{\epsilon}_{33} = 1.8\%$, both with $\sigma_{11} = 0$.

of cells results in a ratio of about 60 between the size of the considered region $2H = 2L$ and the cavity radius a which is sufficiently high.

Applications

In the following applications, results are shown in which an elastoplastic aluminum alloy whose behavior is governed by the incremental classical plasticity, Equation (4), is employed to form the inelastic phase. The parameters of this elastoplastic linear hardening material are given in Table 2.

Figure 3 shows the response of an infinite elastoplastic aluminum alloy in which a cavity of radius $a/(2h) = 0.28$ is embedded. This system is subjected to a far-field uniaxial strain loading which is incrementally applied reaching the final value of $\bar{\epsilon}_{22} = 0.02$ with $\bar{\epsilon}_{11} = 0$. For a transverse traction-free $\bar{\sigma}_{33} = 0$, the component $\bar{\epsilon}_{33}$ is determined at any stage of loading by the HFGMC model for a homogeneous elastoplastic material. This figure shows the elastoplastic variations of the σ_{22} along x_3 at $x_2 = 0$ at the final stage of loading together with the equivalent plastic strain whose increment is given by

$$\Delta \epsilon_{eq}^p = \sqrt{\frac{2}{3}} \Delta \epsilon^p : \Delta \epsilon^p \quad (37)$$

This figure also shows, for a comparison, the corresponding response in the special case of perfectly elastic aluminum. Obviously,

Table 1: The parameters of the Ramberg-Osgood elastoplastic material.

E (GPa)	ν	Y (MPa)	α	n
5.2	0.35	157.6	3/7	4

E , ν , Y , α and n denote the Young's modulus, Poisson's ratio, yield stress and two parameters, respectively.

Table 2: The parameters of the elastoplastic aluminum alloy with linear hardening material.

E (GPa)	ν	Y (MPa)	H (GPa)
68.3	0.3	371.5	23

E , ν , Y and H denote the Young's modulus, Poisson's ratio, yield stress and hardening, respectively.

Table 3: The elastic properties of the boron.

E (GPa)	ν
400	0.2

E and ν denote the Young's modulus and Poisson's ratio, respectively.

up to 0.02 together with $\bar{\epsilon}_{11} = 0$. The stress concentration factor in the elastic case provides the value of about 1.9 as compared to the theoretical value of 2. The corresponding elastoplastic value is seen to be about 1.6.

Finally, the response of the infinite aluminum alloy with embedded cavity which is subjected to a biaxial loading of the form $\bar{\epsilon}_{22} = -\bar{\epsilon}_{33} = 0.02$ with $\bar{\epsilon}_{11} = 0$ is shown in Figure 5. Here, the elastic and elastoplastic stress concentration factors are about 3.9 (theoretically 4) and 3.25, respectively.

The next two applications concern with a periodic unidirectional boron/aluminum metal matrix composite in which one of the elastic boron fibers is either completely lost ($D = 1$) thus forming a cavity, or his Young's modulus deteriorated to one half of its original value ($D = 0.5$). These two situation might caused by a production defect or

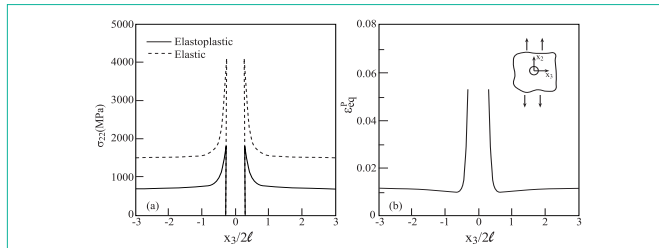


Figure 3: The response along x_3 at $x_2 = 0$ of elastoplastic material with an embedded cavity, subjected to uniaxial strain loading of $\bar{\epsilon}_{22} = 0.02$ with $\bar{\epsilon}_{11} = 0$ and $\bar{\sigma}_{33} = 0$. (a) σ_{22} vs. x_3 , (b) ϵ_{eq}^p vs. x_3 .

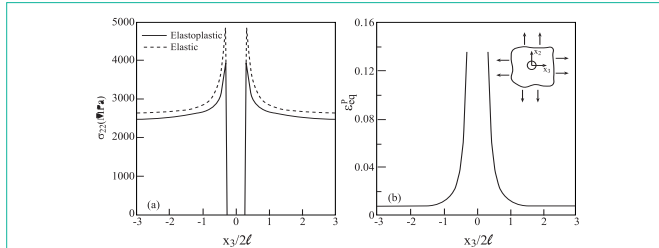


Figure 4: The response along x_3 at $x_2 = 0$ of elastoplastic material with an embedded cavity, subjected to biaxial strain loading of $\bar{\epsilon}_{22} = \bar{\epsilon}_{33} = 0.02$ with $\bar{\epsilon}_{11} = 0$. (a) σ_{22} vs. x_3 , (b) ϵ_{eq}^p vs. x_3 .

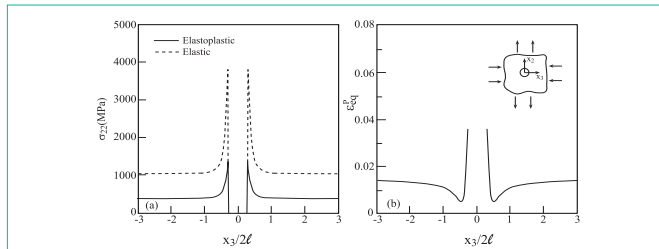


Figure 5: The response along x_3 at $x_2 = 0$ of elastoplastic material with an embedded cavity, subjected to biaxial strain loading of $\bar{\epsilon}_{22} = -\bar{\epsilon}_{33} = 0.02$ with $\bar{\epsilon}_{11} = 0$. (a) σ_{22} vs. x_3 , (b) ϵ_{eq}^p vs. x_3 .

the cavity forms a stress concentrator which in the perfectly elastic case generates a stress concentration factor equal to 3 for normal stress in the loading direction. The ratio between σ_{22} at the edge of the cavity and the far-field $\bar{\sigma}_{22}$ value in this latter case shows that the stress concentration factor is about 2.8 as compared to the theoretical value of 3. As expected, the elastoplastic results predict a far lower value of about 2. The graph of the equivalent plastic strain ϵ_{eq}^p indicates that the intensity of the plastic field is concentrated near the edges of the cavity and decays rapidly away from it.

Similarly, the response to a biaxial strain loading of the infinite aluminum alloy with embedded cavity is shown in Figure 4. Here the far-field strain components $\bar{\epsilon}_{22} = \bar{\epsilon}_{33}$ are incrementally increased

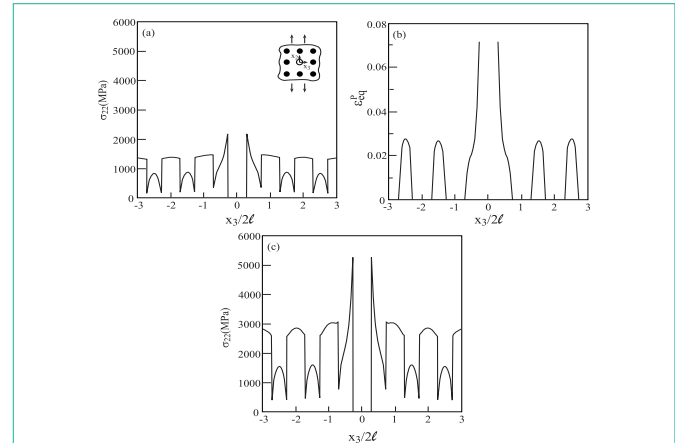


Figure 6: The response along x_3 at $x_2 = 0$ of boron/aluminum elastoplastic composite ($\nu_f = 0.25$) with a missing fiber, subjected to uniaxial strain loading of $\bar{\epsilon}_{22} = 0.02$ with $\bar{\epsilon}_{11} = 0$ and $\bar{\sigma}_{33} = 0$. (a) σ_{22} vs. x_3 , (b) ϵ_{eq}^p vs. x_3 , (c) σ_{22} vs. x_3 assuming perfectly elastic aluminum.

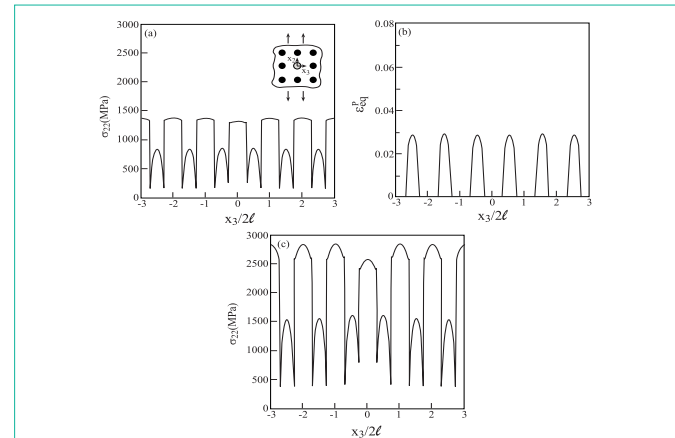


Figure 7: The response along x_3 at $x_2 = 0$ of boron/aluminum elastoplastic composite ($\nu_f = 0.25$) with a half missing fiber, subjected to uniaxial strain loading of $\bar{\epsilon}_{22} = 0.02$ with $\bar{\epsilon}_{11} = 0$ and $\bar{\sigma}_{33} = 0$. (a) σ_{22} vs. x_3 , (b) ϵ_{eq}^p vs. x_3 , (c) σ_{22} vs. x_3 assuming perfectly elastic aluminum.

damage during service. The properties of the boron fibers are given in Table 3 and the fiber volume ratio is $\nu_f = 0.25$. Figure 6(a) shows the variations of σ_{22} along x_3 at $x_2 = 0$ of the boron/aluminum composite with a missing fiber at the final stage of uniaxial strain loading of $\bar{\epsilon}_{22} = 0.02$ with $\bar{\epsilon}_{11} = 0$. The other far-field strain component is determined by the HFGMC modeling of an unperturbed periodic unidirectional boron/aluminum metal matrix composite by imposing the condition that $\bar{\sigma}_{33} = 0$. Figure 6(b) and the corresponding variations of the equivalent plastic strain ϵ_{eq}^p reveal that the effect of missing fiber is confined to the vicinity of the cavity with a rapid decay away from the defect location. Figure 6(c) shows a similar behavior when the aluminum matrix is assumed to be perfectly elastic.

The corresponding response of the boron/aluminum metal matrix composite in which the value of the Young's modulus of a single boron fiber is reduced from 400GPa to 200GPa (e.g., by an imperfect bonding) is shown in Figure 7. The first two parts of this figure indicates that the effect of this defect is quite minor in the elastoplastic case, but Figure 7(c) in which the aluminum alloy is assumed to behave elastically a small stress deterioration can be detected across the defective fiber.

Thus far, the effects of cavities, missing and partially missing fibers have been investigated. Presently, the effect of cracks in homogeneous, fiber reinforced and layered metal matrix composites are addressed.

Consider a single crack in the infinite aluminum alloy which is subjected to a far-field uniaxial strain $\bar{\epsilon}_{22} = 0.02$ with $\bar{\epsilon}_{11} = 0$ and $\bar{\sigma}_{33} = 0$. The length of the crack is $2a/(2l) = 0.5$. The resulting σ_{22} and ϵ_{eq}^p variations along the crack line x_3 at $x_2 = 0$ are shown in Figure 8(a) and (b).

Also shown is the response in the special case when the aluminum is assumed to be perfectly elastic. Here an analytical solution is

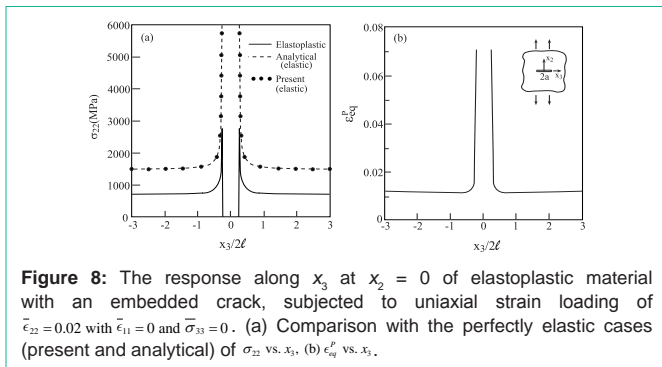


Figure 8: The response along x_3 at $x_2 = 0$ of elastoplastic material with an embedded crack, subjected to uniaxial strain loading of $\bar{\epsilon}_{22} = 0.02$ with $\bar{\epsilon}_{11} = 0$ and $\bar{\sigma}_{33} = 0$. (a) Comparison with the perfectly elastic cases (present and analytical) of σ_{22} vs. x_3 , (b) ϵ_{eq}^p vs. x_3 .

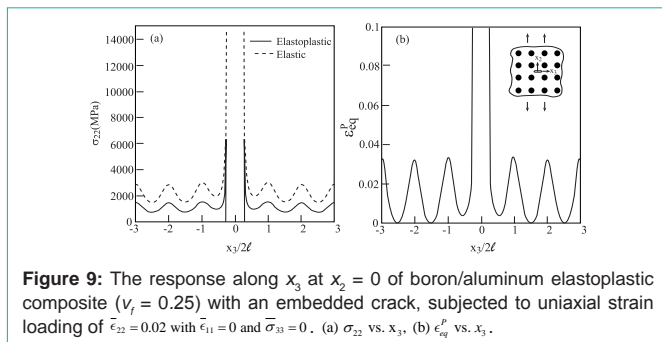


Figure 9: The response along x_3 at $x_2 = 0$ of boron/aluminum elastoplastic composite ($\nu_f = 0.25$) with an embedded crack, subjected to uniaxial strain loading of $\bar{\epsilon}_{22} = 0.02$ with $\bar{\epsilon}_{11} = 0$ and $\bar{\sigma}_{33} = 0$. (a) σ_{22} vs. x_3 , (b) ϵ_{eq}^p vs. x_3 .

available, e.g. Sneddon [12], which is compared with the prediction of the present approach in this special elastic case. This comparison reveals an excellent agreement. The reduction of the magnitude of the stress in the vicinity of the crack's tip in the elastoplastic case is well observed and the sharp high values of the plastic strains there is shown in Figure 8(b).

The next application concerns with the periodic boron/aluminum metal matrix composite ($\nu_f = 0.25$) with an embedded crack of length $2a/(2l) = 0.6$ along the x_3 -axis within the aluminum matrix. The composite is subjected to a far-field uniaxial strain $\bar{\epsilon}_{22} = 0.02$ with $\bar{\epsilon}_{11} = 0$. As discussed, the other strain component is determined by the HFGMC by imposing the condition $\bar{\sigma}_{33} = 0$. The resulting variations of σ_{22} and ϵ_{eq}^p along the crack's line are shown in Figure 9(a) and (b), respectively. Also shown in Figure 9(a) is the

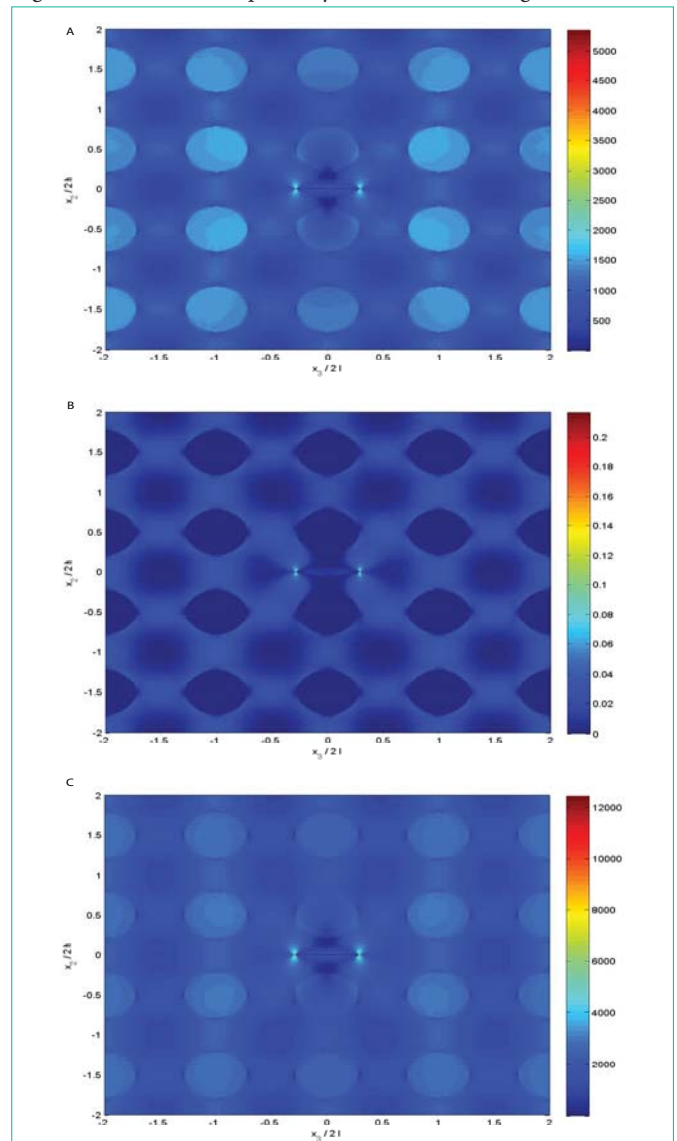


Figure 10: Field distribution of boron/aluminum elastoplastic composite ($\nu_f = 0.25$) with an embedded crack in the region $-2 \leq x_2/(2h) \leq 2$, $-2 \leq x_3/(2l) \leq 2$. The composite is subjected to uniaxial strain loading of $\bar{\epsilon}_{22} = 0.02$ with $\bar{\epsilon}_{11} = 0$ and $\bar{\sigma}_{33} = 0$. (a) The distribution of the equivalent stress σ_{eq}^p , (b) of the equivalent strain ϵ_{eq}^p and (c) The distribution of the equivalent stress σ_{eq} assuming a perfectly elastic aluminum.

Table 4: The elastic properties of the Al_2O_3 ceramic material.

$E(\text{GPa})$	ν
380	0.2

E and ν denote the Young's modulus and Poisson's ratio, respectively.

corresponding variation when the aluminum is assumed to behave as a perfectly elastic material. The reduction of the magnitude of the stress in crack's tip as compared to elastic case is noticeable. The equivalent plastic strain reaches the value of 0.22 (not shown in the figure) rendering the employed infinitesimal plasticity theory questionable there.

It should be interesting to show the distribution of the equivalent stress σ_{eq} and plastic strain ϵ_{eq}^p in the vicinity of the crack. These are shown in Figure 10(a) and (b), respectively, in the region $-2 \leq x_2/(2h) \leq 2, -2 \leq x_3/(2l) \leq 2$. These two figures well display the resulting effect of the crack on its surrounding region of fibers and matrix. For comparison, Figure 10(c) shows the corresponding equivalent stress distribution when the aluminum matrix is assumed to behave elastically. Note that the scale of the plot is twice the scale of the elastoplastic case.

Our last application of the present theory concerns with the effect of a broken ceramic layer in periodically ceramic/aluminum layered composite. The elastic Al_2O_3 ceramic layer is characterized in Table 4. The composite is subjected to a far-field uniaxial strain $\bar{\epsilon}_{22} = 0.02$ with $\bar{\epsilon}_{11} = 0$ and other applied strain component is determined by the HFGMC analysis by imposing the condition $\bar{\sigma}_{33} = 0$. Comparisons between the variations of σ_{22} along the crack's line are shown in Figure 11 of the elastoplastic and elastic cases. In this figure, the widths of the ceramic and aluminum layer are equal so that the crack's length is $2a/(2l) = 0.5$.

Let us consider a very thin aluminum layer such that the length of the crack in the broken ceramic layer is $2a/(2l) = 0.95$. The resulting comparison between the variations of σ_{22} along the crack's line is shown in Figure 12(a) for the elastoplastic and elastic aluminum layer. More interesting is distribution of the equivalent plastic strain ϵ_{eq}^p in the region $-2 \leq x_2/(2h) \leq 2, -2 \leq x_3/(2l) \leq 2$. This is shown in Figure 12(b) where ϵ_{eq}^p reaches the value of 0.45 in the vicinity of the crack's tip. In addition, the spread of plasticity over quite an extended region along the aluminum layer is notable.

Asymptotic fracture analysis of the considered case of a very

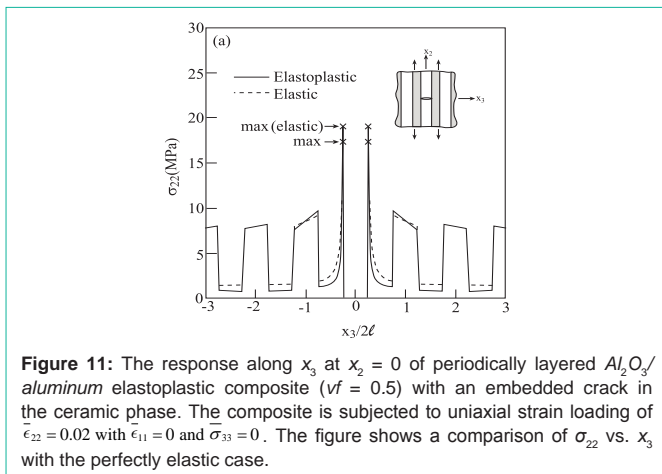


Figure 11: The response along x_3 at $x_2 = 0$ of periodically layered Al_2O_3 /aluminum elastoplastic composite ($\nu_f = 0.5$) with an embedded crack in the ceramic phase. The composite is subjected to uniaxial strain loading of $\bar{\epsilon}_{22} = 0.02$ with $\bar{\epsilon}_{11} = 0$ and $\bar{\sigma}_{33} = 0$. The figure shows a comparison of σ_{22} vs. x_3 with the perfectly elastic case.

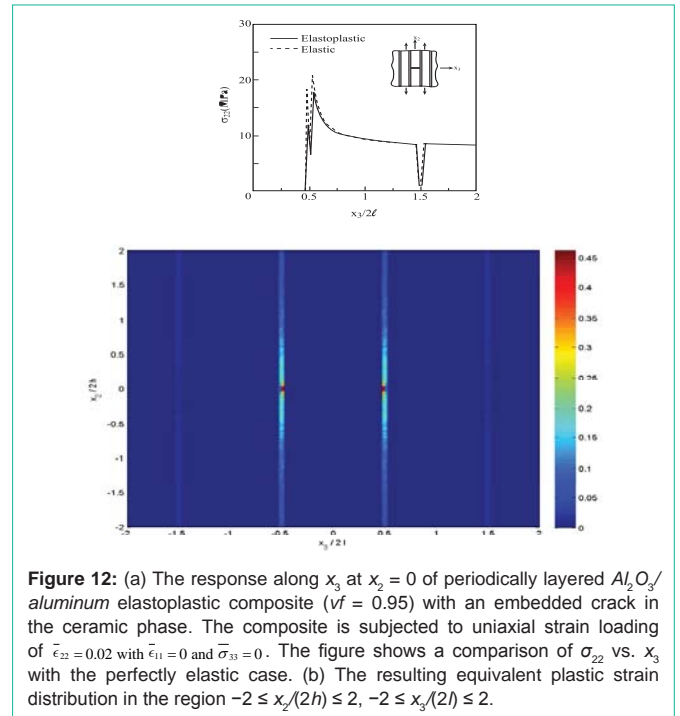


Figure 12: (a) The response along x_3 at $x_2 = 0$ of periodically layered Al_2O_3 /aluminum elastoplastic composite ($\nu_f = 0.95$) with an embedded crack in the ceramic phase. The composite is subjected to uniaxial strain loading of $\bar{\epsilon}_{22} = 0.02$ with $\bar{\epsilon}_{11} = 0$ and $\bar{\sigma}_{33} = 0$. The figure shows a comparison of σ_{22} vs. x_3 with the perfectly elastic case. (b) The resulting equivalent plastic strain distribution in the region $-2 \leq x_2/(2h) \leq 2, -2 \leq x_3/(2l) \leq 2$.

thin elastoplastic layers sandwiched between brittle elastic ones was performed by Chan et al. [13]. In this latter work a transverse crack in an elastic layer of thickness $2w$ was terminated at the plastic zone which was modeled by open or closed cracks of length $2d$ developed within elastoplastic layers, thus forming an H-crack configuration. It was found, in particular, that in the case of shear traction-free closed cracks in the plastic zone of the size characterized by the ratio $d/w = 0.5$, the stress concentration factor for the tensile stresses in the brittle layer adjacent to the cracked one is about 2. Inspection of the results in Figure 12 obtained in the present investigation shows that they confirm with Chan et al. [13] finding.

Conclusion

A method for the modeling of localized damage in elastoplastic composites with periodic microstructure has been presented. As a result of the localization effects (perturbations) the periodicity is lost and a repeating unit cell cannot be identified anymore. The method is based on the combination of three distinct types of analyses, namely the representative cell method, the higher-order theory for inelastic composites and the high-fidelity generalized method of cells micromechanical analysis which is needed for the determination of the far-field boundary conditions.

The representative cell method has been previously applied to solve linear and nonlinear problems, but the present method enables for the first time the analysis of elastoplastic materials. To this end, the plasticity effects are represented in the form of eigenstresses which are distributed over the entire region. In addition, these eigenstresses include the perturbation effects which are distributed over the damaged regions. The method has been applied in various cases for the prediction of the field distributions in elastoplastic materials and metal matrix composites with fiber loss and crack. Finally, the elastoplastic field in ceramic/aluminum layered composite in which a

single ceramic layer is broken has been determined. Results confirm with a previously derived asymptotic analysis [13]. Presently, results for normal loading have been presented. Shear loading can be carried out in the same manner.

The present approach can be extended to the analysis of elastic-viscoplastic composites with a localized damage by changing the flow rule of the elastoplastic matrix, Equation (4), to a viscoplastic one. In addition, although the present analysis has been confined to isothermal conditions, the inclusion of temperature effects in the eigenstresses can be easily performed, see Ryvkin and Aboudi [5] for the case of H-cracks in thermoelastic composites. Another possible generalization is to allow the damage to evolve with the applied loading. Thus instead of applying an a priori a constant damage (e.g., $D = 0.5$ in the previously discussed case of a boron fiber with a reduced Young's modulus), an evolution law can be adopted which according to Lemaitre and Desmorat [10] has the form

$$\Delta D = \left(\frac{y}{S} \right)^s \Delta \epsilon_{eq}^p \quad (38)$$

where y is the energy release, S and s are material parameters. Finally, extension to inelastic metal matrix composites with triply periodic microstructure (short-fiber composites) which include localized damage that appears in several locations is possible.

Acknowledgment

The first author is grateful for the support of the German-Israel Foundation (GIF) under contract 1166-163.

References

1. Aboudi J, Ryvkin M. The effect of localized damage on the behavior of composites with periodic microstructure. *Int J Engng Sci.* 2012; 52: 41-55.
2. Ryvkin M, Nuller B. Solution of quasi-periodic fracture problems by the representative cell method. *Comp Mech.* 1997; 20: 145-149.
3. Aboudi J, Ryvkin M. The analysis of localized effects in composites with periodic microstructure. *Philos Trans A Math Phys Eng Sci.* 2013; 371: 20120373.
4. Aboudi J, Arnold SM, Bednarczyk BA. *Micromechanics of Composite Materials: A Generalized Multiscale Analysis Approach.* Elsevier, Oxford, UK. 2013.
5. Ryvkin M, Aboudi J. Stress redistribution due to cracking in periodically layered composites. *Eng Fract Mech.* 2012; 93: 225-238.
6. Aboudi J. Field distributions in cracked periodically layered electro-magneto-thermo-elastic composites. *J Intell Mater Sys Struct.* 2012; 24: 381-398.
7. Aboudi J. The effect of localized internal defects on the field distributions of electrostrictive composites. *Int J Engng Sci.* 2014; 75: 135-153.
8. Ishikawa H. Stresses in the plastic range around a circular hole in an infinite sheet subjected to equal biaxial tension. *J Appl Math Mech (ZAMM).* 1975; 55: 171-178.
9. Mendelson A. *Plasticity: Theory and Applications,* MacMillan, New York. 1968.
10. Lemaitre J, Desmorat R. *Engineering Damage Mechanics,* Springer, Berlin. 2005.
11. Budiansky B, Mangasarian OL. Plastic stress concentration at a circular hole in an infinite sheet subjected to equal biaxial tension. *J Appl Mech.* 1960; 27: 59-64.
12. Sneddon IN. *Fourier Transforms.* McGraw Hill, New York. 1951.
13. Chan KS, He MY, Hutchinson JW. Cracking and stress redistribution in ceramic layered composites, *Mater. Sci Eng.* 1993; A167: 57-64.